**Showcasing research from Professor Gangishetty's laboratory, Department of Chemistry, Mississippi State University, Mississippi, USA.**

Interstitial and substitutional doping of $Mn^{2+}$ in 2D $PEA_2PbBr_4$ and $BA_2PbBr_4$ perovskites

This work provides comprehensive structural analyses of the type of $Mn^{2+}$ doping, interstitial *vs.* substitutional, in 2D $PEA_2PbBr_4$ and 2D $BA_2PbBr_4$ perovskite hosts. Furthermore, the doping type is linked to optical properties such as exciton diffusion and dopant-to-host energy transfer.

ROYAL SOCIETY
OF **CHEMISTRY**

# rsc.li/chemcomm

Check for updates

# Interstitial and substitutional doping of $Mn^{2+}$ in 2D $PEA_2PbBr_4$ and $BA_2PbBr_4$ perovskites†

Udara M. Kuruppu, [ID] [a] Alvaro J. Magdaleno, [cd] Anuraj S. Kshirsagar, [ID] [a] Bruno Donnadieu, [a] Ferry Prins [ID] *[cd] and Mahesh K. Gangishetty [ID] *[ab]

**$Mn^{2+}$ doping imposes intriguing optoelectronic properties on lead-halide perovskites; however, its impact on their crystal structure remains unclear. This study investigates the consequences of interstitial and substitutional $Mn^{2+}$ doping on the lattice-strain and interplanar spacings of 2D perovskites and correlates the structural changes to their optical properties.**

Doping with a foreign metal ion is an attractive strategy to improve the properties of semiconductors such as lead-halide perovskites. Due to the flexible nature of perovskite structures, a wide range of metal ions have been explored. Among these, $Mn^{2+}$ has been most extensively studied due to its bright characteristic emission and paramagnetic nature.[1,2] Despite these extensive studies, the nature of $Mn^{2+}$ doping such as interstitial or substitutional, and the role of host lattice on the doping is still ambiguous. There have been several contradicting results reported on the type of $Mn^{2+}$ doping. Some reports showed lattice contraction due to substitutional $Mn^{2+}$ doping, while others demonstrated lattice expansion owing to their interstitial nature. Generally, the lattice expansion and contraction can be identified by the shift in their p-XRD peaks. Recently, Torma *et al.* observed a shift in the XRD peak to lower angles and demonstrated interstitial $Mn^{2+}$ doping in $Cs_2PbI_2Cl_2$ using nano-XRD and nano-XRF measurements.[3] On the contrary, Dutta *et al.* and Hou *et al.* observed a peak shift to the higher angles in XRD after doping with $Mn^{2+}$ in 2D $Cs_2PbBr_4$ nanoplatelets and 3D $CsPb(BrCl)_3$ perovskite nanocrystals.[4,5] Interestingly, Nag *et al.* observed no shift in the XRD peak when

$Mn^{2+}$ ($<1\%$) is doped in 2D $BA_2PbBr_4$ perovskite.[6] Therefore, a comprehensive understanding of the nature of doping, its dependence on the host lattice structure, and its impact on the crystal structure, lattice strain, and optical properties of perovskites is required.

In this study, we utilize $Mn^{2+}$ doping in two different 2D perovskite hosts: (i) phenylethylammonium lead bromide ($PEA_2PbBr_4$) and (ii) butylammonium lead bromide ($BA_2PbBr_4$), to investigate their structural changes and link these changes to their optical properties. These two perovskites are selected by considering the difference in their structural rigidity owing to the difference in their A-site ions, although both adopt similar layered 2D structures of the Ruddlesden–Popper (RP) type.[7] Consequently, our study reveals that the nature of $Mn^{2+}$ doping is significantly different in both $PEA_2PbBr_4$ and $BA_2PbBr_4$. We observed a striking difference in their XRD patterns after $Mn^{2+}$ doping. $PEA_2PbBr_4$ showed lattice expansion perpendicular to the plane of the 2D inorganic framework (interstitial nature) after doping with $Mn^{2+}$ whereas $BA_2PbBr_4$ showed a lattice contraction along the 2D plane (substitutional doping). Due to the manifestation of a soft lattice with a layered structure of 2D perovskites, the $Mn^{2+}$ doping was feasible, and the changes in their crystal structure were easily noticeable after $Mn^{2+}$ incorporation. Subsequently, this resulted in a dramatic difference in their emission; orange ($Mn^{2+}$) emission in $Mn^{2+}:PEA_2PbBr_4$ is more intense ($\sim 10\times$ higher) than that of $Mn^{2+}:BA_2PbBr_4$. Upon tracking the exciton diffusion using transient photoluminescence microscopy (TPLM), we found that the exciton transport in $PEA_2PbBr_4$ is unaffected, whereas a noticeable difference in the exciton transport was observed in $BA_2PbBr_4$ with $Mn^{2+}$ doping.

To commence our study, undoped and a series of $Mn^{2+}$ doped 2D perovskites were synthesized using acid-initiated precipitation (detailed methodology is available in the ESI†). The ICP-MS analyses reveal that the amount of $Mn^{2+}$ increases with an increase in the concentration of $Mn^{2+}$ salts in the precursors (shown in Table S3, ESI†). However, the maximum feasible doping amount was 4.8% and 2.0% of $Mn^{2+}$ (respective to the molar percentage of $Pb^{2+}$) for $PEA_2PbBr_4$ and $BA_2PbBr_4$, respectively. Such low

*[a] Department of Chemistry, Mississippi State University, Mississippi State, Mississippi 39762, USA. E-mail: mg2234@msstate.edu*

*[b] Department of Physics and Astronomy, Mississippi State University, Mississippi State, Mississippi 39762, USA*

*[c] Condensed Matter Physics Center (IFIMAC), Autonomous University of Madrid, 28049, Madrid, Spain. E-mail: ferry.prins@uam.es*

*[d] Department of Condensed Matter Physics, Autonomous University of Madrid, 28049, Madrid, Spain*

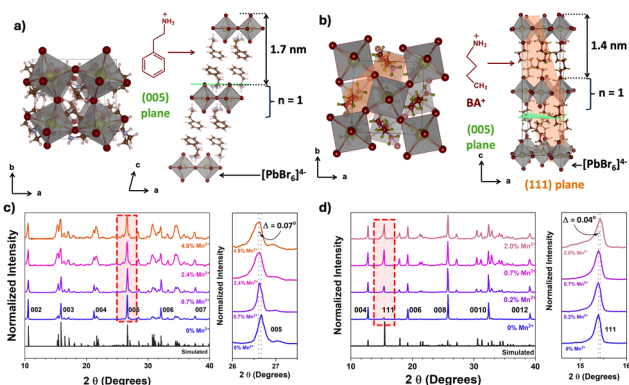† Electronic supplementary information (ESI) available. See DOI: https://doi.org/10.1039/d4cc04074k

Fig. 1 Crystal structures of (a) $PEA_2PbBr_4$ and (b) $BA_2PbBr_4$. The pXRD patterns of undoped and $Mn^{2+}$ doped (c) $PEA_2PbBr_4$ and (d) $BA_2PbBr_4$. The 2D perovskite lattices of $PEA_2PbBr_4$ and $BA_2PbBr_4$ are composed of a single ($n$ = 1) inorganic layer of $[PbBr_6]^{4-}$ octahedra. The $PEA^+$ and $BA^+$ cations act as organic spacers between the octahedral layers of $PEA_2PbBr_4$ and $BA_2PbBr_4$, respectively.

doping levels of $Mn^{2+}$ are attributed to a difference in the ionic radii of $Mn^{2+}$ (0.83 Å) compared to that of $Pb^{2+}$ (1.19 Å).[6,8] The crystal structures of $PEA_2PbBr_4$ and $BA_2PbBr_4$ were analyzed by scXRD and shown in Fig. 1a and b (see Tables S1 and S2 for refined data, ESI†). Both perovskites show 2D layered Ruddlesden–Popper (RP) type structures and exhibit a higher degree of preferential orientation along the $c$-axis. Further, their p-XRD patterns were recorded after doping with various amounts of $Mn^{2+}$ (Fig. 1c and d), which was and used for strain analyses. From p-XRD, we found that both perovskites retain the RP structures even after doping with $Mn^{2+}$.

In the case of $PEA_2PbBr_4$, both undoped and $Mn^{2+}$ doped perovskites show equally spaced and sharp diffraction peaks in p-XRD (Fig. 1c), denoted as (002), (003), (004), *etc.*, and agree with the simulated pattern of a triclinic phase (lattice parameters $a \neq b \neq c$, $\alpha \neq \beta \neq \gamma$) derived from scXRD. All these peaks arise from the same family of planes $\{00l\}$ where ($l = n$), indicating the high degree of orientation with stacking layers. The periodic peaks due to these (00$l$) diffractions imply the spacing between the two layers, since these planes are perpendicular to the stacking axis ($c$-axis), see Fig. 1a. The periodicity obtained from the diffraction peaks was 1.648 ± 0.007 nm, indicating that each layer is ∼1.65 nm apart, as shown in Fig. 1a. After doping with $Mn^{2+}$, no major changes in the p-XRD pattern were observed; however, a shift in some XRD peaks with slight broadening was observed. These peaks are at ∼26.6° and at ∼37.6°, which correspond to the (005) plane and the (007) plane, respectively, as shown in the magnified region of Fig. 1c and Fig. S1 (ESI†). The magnitude of the shift was $\Delta 2\theta_{005}$ = 0.07° and $\Delta 2\theta_{007}$ = 0.09°. Generally, given the difference in the ionic radii of $Pb^{2+}$ (1.19 Å) and $Mn^{2+}$ (0.83 Å), if $Pb^{2+}$ is replaced by smaller $Mn^{2+}$, a lattice contraction is expected with a shift in the XRD peaks to higher angular scale. On the contrary, in this case, the XRD peaks shifted to lower angles, indicating that there is a lattice expansion after doping with $Mn^{2+}$ ions. This also implies that the $Mn^{2+}$ ions are not replacing $Pb^{2+}$. Since this shift is observed for (005) and (007) peaks, the lattice expansion occurs in an out-of-plane direction

(perpendicular to (005) and (007) planes) along the $c$-axis, as shown in Fig. 1a. This is also evident from an increase in the spacing of (005) planes, as shown in Fig. 2a. Similar trends in p-XRD were observed by Torma *et al.*[3] By using nano-XRD, they demonstrated that $Mn^{2+}$ occupies the interstitial position.[3]

In the case of 2D $BA_2PbBr_4$, the powder XRD patterns of both undoped and $Mn^{2+}$ doped show equally spaced and sharp diffraction peaks indexed as (002), (004), (006), *etc* (Fig. 1d). This diffraction pattern aligns well with the simulated pattern obtained from the reference and scXRD data, confirming the orthorhombic Ruddlesden–Popper crystal structure (lattice parameters $a \neq b \neq c$, $\alpha = \beta = \gamma = 90°$). All these peaks arise from the same family of planes $\{00l\}$, where ($l = 2n$) indicates highly oriented crystallites. The periodicity, obtained from $\{00l\}$ family peaks, was found to be 1.366 ± 0.008 nm. Note that this interlayer spacing is smaller than the spacing in $PEA_2PbBr_4$ perovskite. Unlike $PEA_2PbBr_4$, neither a peak shift nor broadening of the (00$l$) planes was observed upon doping, indicating these planes are unaffected after the incorporation of $Mn^{2+}$ in $BA_2PbBr_4$. Interestingly, in addition to the (00$l$) family peaks, another peak at ∼15.5°, corresponds to the (111) plane, was observed (Fig. 1d). This (111) plane cuts the organic and inorganic layers diagonally, as shown in Fig. 1b.[9] Upon a close examination, a slight shift in the ∼15.5° peak to higher angles was observed (magnified region of Fig. 1d). This shift was more prominent at higher (>1%) $Mn^{2+}$ doping, and almost negligible at lower doping levels. The magnitude of this shift was $\Delta 2\theta$ = 0.04°. The shift in this peak to higher angular scale implies there is a lattice contraction along the out-of-plane direction along the $ab$-plane (perpendicular to the (111) plane and the $c$-axis), as shown in Fig. 1b. This is further corroborated by the decrease in $d$-spacing of (111) planes, as shown in Fig. 2b. From the crystal structure in Fig. 1b, this $ab$ plane represents the plane of the inorganic framework; the lattice contraction along this plane implies that there is shrinkage of the inorganic framework. This is possible only when the central atom, $Pb^{2+}$, is replaced by an atom with a smaller ionic radius such as $Mn^{2+}$. Therefore, from these analyses, it is evident that the $Mn^{2+}$ in $BA_2PbBr_4$ is substituting $Pb^{2+}$, whereas, in the case of $PEA_2PbBr_4$, the $Mn^{2+}$ is occupying interstitial sites.[6,10] This difference in occupancy, despite the similar layered RP type structure, could be attributed to either the smaller interlayer spacing in $BA_2PbBr_4$ compared to $PEA_2PbBr_4$ or a difference in the lattice
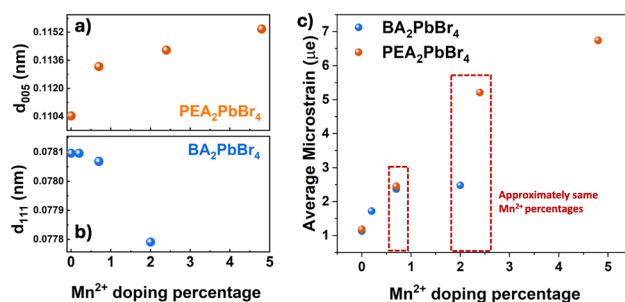


Fig. 2 The change in $d$-spacing against $Mn^{2+}$ concentration of (a) the (005) plane in $PEA_2PbBr_4$ (b) the (111) plane in $BA_2PbBr_4$ and (c) microstrain *vs.* $Mn^{2+}$ doping percentage.

rigidity owing to difference in their organic spacers (aromatic *vs.* aliphatic). Perhaps this substitutional nature of $Mn^{2+}$ doping is limiting the amount of $Mn^{2+}$ that can be incorporated into $BA_2PbBr_4$, since a maximum of only ~2% doping was achievable synthetically.

Regardless of the crystal phases, type of spacers, and interstitial or substitutional doping, the incorporation of $Mn^{2+}$ into the perovskite host can induce strain in the lattice. Generally, from the changes in the p-XRD peaks, one can estimate the strain in the lattice. A peak shift with a slight broadening in $PEA_2PbBr_4$ after $Mn^{2+}$ doping may be an indication of a homogenous strain caused by the uniform expansion of the lattice. Whereas a moderate change in peak position in the case of $BA_2PbBr_4$, suggesting that the magnitude of the lattice strain is less in the case of $BA_2PbBr_4$.[11] To quantitatively compare the microstrain induced by $Mn^{2+}$ incorporation in these two host lattices, we employed the Williamson–Hall method (Fig. S2, ESI†).[12] A Voigt function, which is convoluted Lorentzian and Gaussian functions, was used to fit the p-XRD peaks and derive the FWHM for the strain analyses. From Fig. 2c, a striking difference in the microstrain was observed at higher $Mn^{2+}$ levels. At >2% of $Mn^{2+}$ doping, the strain in the $PEA_2PbBr_4$ is approximately three times higher than that of $BA_2PbBr_4$, implying that the interstitial doping can induce more strain in the lattice than the substitutional doping.

Next, the impact of these discrepancies in the $Mn^{2+}$ occupancy on the optical properties of perovskites was investigated. We recorded absorption, photoluminescence (PL), and exciton diffusion in $PEA_2PbBr_4$ and $BA_2PbBr_4$ perovskites with and without $Mn^{2+}$ doping. As shown in Fig. S3 (ESI†), both pristine perovskites exhibit sharp excitonic features in the UV-vis absorption spectra with similar band-edge absorption at 2.89 eV (430 nm) for $PEA_2PbBr_4$ and at 2.85 eV (435 nm) for $BA_2PbBr_4$ (Fig. S4, ESI†). The absorbance remains unchanged upon $Mn^{2+}$ doping of the pristine 2D perovskites. Supporting this, we observed no change in the excitation (PLE) spectra after $Mn^{2+}$ doping (Fig. S6, ESI†). The PL spectra of both pristine 2D perovskites exhibit two emission features around 410 nm and 430 nm, similar to other studies.[13] As these are 2D layered perovskites, the lower energy peak at 430 nm is due to the recombination of edge excitons, while the higher energy transition at 410 nm is designated to interior excitons.[10,13] When $Mn^{2+}$ is introduced into both $BA_2PbBr_4$ and $PEA_2PbBr_4$, a new broad, intense emission at 600 nm was observed. This 600 nm emission has been assigned to $^4T_{1g} \rightarrow {}^6A_{1g}$ d–d transition in $Mn^{2+}$.[6,10] These Mn states are typically sensitized from the host's excitation, and the emission originates from the excitonic energy transfer from the host to the dopant ion (Fig. S5, ESI†).[6] Interestingly, the intensity of the $Mn^{2+}$ peak (600 nm) with respect to the host peak (~430 nm) is significantly different in $Mn^{2+}:BA_2PbBr_4$ compared to $Mn^{2+}:PEA_2PbBr_4$ (Fig. S7, ESI†); this is true even in the case of samples with the same amount of $Mn^{2+}$ (Fig. S13, ESI†). For instance, the PL intensity ratio between dopant and host emission in ~2% $Mn^{2+}$-doped $PEA_2PbBr_4$ suggests an equal intensity dopant peak with the host. Whereas in $BA_2PbBr_4$, at the same $Mn^{2+}$ loading, the intensity of the dopant peak was only ~1/4th of the host peak (Fig. S7, ESI†). Consequently, under the 365 nm excitation, the color of $Mn^{2+}:PEA_2PbBr_4$ crystals
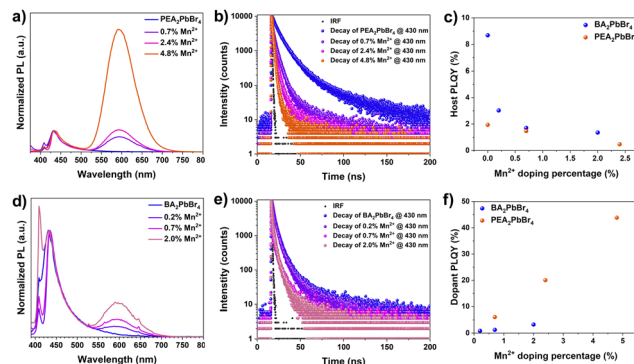


Fig. 3 (a) PL spectra of $Mn^{2+}:PEA_2PbBr_4$. (b) TRPL of $Mn^{2+}:PEA_2PbBr_4$. (c) Host PLQY against $Mn^{2+}$ percentage. (d) PL spectra of $Mn^{2+}:BA_2PbBr_4$. (e) TRPL of $Mn^{2+}:BA_2PbBr_4$. (f) Dopant PLQY against $Mn^{2+}$ percentage.

appeared significantly different from $Mn^{2+}:BA_2PbBr_4$ (Fig. S9–S11, ESI†). The emission color tends to move towards orange ($\lambda_{Em}$ = 600 nm) in $Mn^{2+}:PEA_2PbBr_4$; however, a more prominent blue emission in $Mn^{2+}:BA_2PbBr_4$ was observed. These deviations in the PL spectra of $Mn^{2+}:BA_2PbBr_4$ and $Mn^{2+}:PEA_2PbBr_4$ crystals show a clear distinction in the CIE 1931 (Commission Internationale de l'Eclairage) chromaticity diagram in Fig. S14 (ESI†).

Furthermore, the time-resolved photoluminescence (TRPL) was recorded at 430 nm and 435 nm for both undoped $PEA_2PbBr_4$ and $BA_2PbBr_4$ on the order of nanoseconds (Fig. 3c, and f). The average lifetimes decrease with an increase in $Mn^{2+}$ levels, as shown in Tables S4 and S5 (ESI†). Under the same excitation fluence, the average lifetime of undoped $PEA_2PbBr_4$ (~8.2 ns) is significantly higher than undoped $BA_2PbBr_4$ (~3 ns). With a small amount of $Mn^{2+}$ doping, there is a dramatic decrease in the lifetime of the $PEA_2PbBr_4$ when compared to $BA_2PbBr_4$, indicating an efficient host-dopant energy transfer in $Mn^{2+}:PEA_2PbBr_4$. This also complements the intense $Mn^{2+}$ PL in $Mn^{2+}:PEA_2PbBr_4$ compared to $Mn^{2+}:BA_2PbBr_4$. Subsequently, the PLQY of the host is decreased (Fig. 3c) and the $Mn^{2+}$ is increased with an increase in the $Mn^{2+}$ doping (Fig. 3f). Both the $Mn^{2+}$ doped 2D perovskites showed a similar decay profile with a prolonged lifetime on the order of microseconds (Fig. S8, ESI†) regardless of the host structure due to the forbidden nature of $Mn^{2+}$ d–d ($^4T_{1g} \rightarrow {}^6A_{1g}$) transitions.[10] As expected, the $PLQY_{Mn}$ of this $Mn^{2+}$ emission at 600 nm increased with an increase in the $Mn^{2+}$ doping in both $PEA_2PbBr_4$ and $BA_2PbBr_4$. However, this increase in $PLQY_{Mn}$ is more prominent in $PEA_2PbBr_4$ compared to $BA_2PbBr_4$, reaching a maximum of 43.8% (Fig. 3f). From all these studies, it is evident that the host-to-dopant ion energy transfer is more efficient in the case of $Mn^{2+}:PEA_2PbBr_4$ compared to $Mn^{2+}:BA_2PbBr_4$. Such differences in optical properties hints towards the important contributions from the nature of doping. In addition, the difference in their crystal phases, and the lattice rigidity due to the difference in their organic spacers may play a critical role in the energy transfer. Regardless, introducing foreign $Mn^{2+}$ ions into the lattice can further perturb the host structure, consequently, the dynamics of exciton transport and the host-to-dopant energy transfer can be affected. After photoexcitation, the excitons generated in the host perovskites diffuse within the inorganic framework before they get
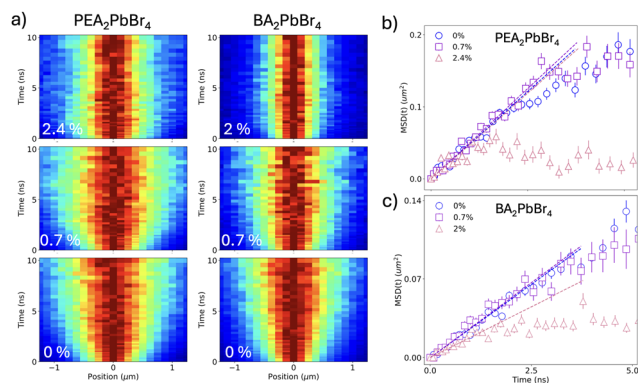
**Fig. 4** (a) Diffusion maps of undoped and $Mn^{2+}$ doped $PEA_2PbBr_4$ and $BA_2PbBr_4$. The extracted mean-square displacement as a function of time for (b) $PEA_2PbBr_4$ and (c) $BA_2PbBr_4$ with different doping levels.

trapped in the $Mn^{2+}$ states. Therefore, the nature of doping, the location of the dopant ions, and strain in the inorganic framework play a critical role in exciton diffusion and energy transport dynamics.[14,15] The efficient host-dopant energy transfer despite the greater strain in $Mn^{2+}$:$PEA_2PbBr_4$ perovskites could be due to either (i) the interstitial doping facilitating the smooth sailing of excitons without affecting the landscape of 2D inorganic framework or (ii) the energy transfer barrier for $Mn^{2+}$ may be lower in $Mn^{2+}$:$PEA_2PbBr_4$. The weak $Mn^{2+}$ emission in the case of $Mn^{2+}$:$BA_2PbBr_4$ perhaps due to the strain created within the inorganic framework due to the lattice contraction by substitutional doping. This strain may be affecting the exciton transport by creating non-radiative defects caused by an inhomogeneous landscape. Consequently, these excitons decay non-radiatively before reaching $Mn^{2+}$ states. Also, the difference in contribution towards the non-radiative sites from rigid aromatic PEA cations and labile aliphatic BA cations cannot be ruled out.

To unveil these dynamics and study the impact of the different doping nature of the two perovskites on exciton transport, we employ TPLM, which allows for direct visualization of in-plane exciton transport. For this, we specifically chose $Mn^{2+}$-doped $PEA_2PbBr_4$ and $BA_2PbBr_4$ with comparable $Mn^{2+}$ doping percentages. Fig. 4a shows the resulting diffusion maps of the undoped and $Mn^{2+}$ doped materials. For both undoped perovskites (Fig. 4a, lower panels), fast spatial expansion of the initial exciton population is observed. In contrast, for doped perovskites, the initial fast diffusion is followed by a stagnation of the expansion, consistent with excitons reaching dopant sites and undergoing energy transfer. We can quantify the rate of expansion by fitting the variance $\sigma$ of the population for each time slice and calculating the mean-square displacement ($MSD(t) = \sigma_t^2 - \sigma_{0-}$), as shown for the different doping levels in Fig. 4b and c for $PEA_2PbBr_4$ and $BA_2PbBr_4$, respectively. From the early time dynamics ($t < 1$ ns), we can extract the diffusivity of the exciton population in the lattice ($MSD = 2D_t$), as indicated by the dashed lines in Fig. 4b and c. For the undoped cases, we observe a higher diffusivity for $PEA_2PbBr_4$ (0.22 cm$^2$ s$^{-1}$) compared to $BA_2PbBr_4$ (0.13 cm$^2$ s$^{-1}$). This is consistent with earlier reports and can be explained by the difference in the softness of the inorganic lattice and a stron-

ger exciton–phonon coupling in $BA_2PbBr_4$, which slows down transport.[16] Upon doping, it is interesting to note that the diffusivity $PEA_2PbBr_4$ remains unaffected (Fig. 4b). In contrast, the expansion is notably slower for the highest (2%) doping concentration in $BA_2PbBr_4$, where the diffusivity drops to 0.08 cm$^2$ s$^{-1}$. Interestingly the same sample, $BA_2PbBr_4$ with 2% $Mn^{2+}$ doping, showed more prominent peak shift in the p-XRD owing to the lattice distortions along the inorganic 2D framework, highlighting the important role of lattice distortions in the exciton diffusion. Further, the lower diffusivity in $BA_2PbBr_4$ can partially explain the lower PLQY of the $Mn^{2+}$ doping in that system, with slower diffusion leading to less efficient energy transfer.

In conclusion, $Mn^{2+}$ doping induces distinct structural changes by occupying different preferential sites in $PEA_2PbBr_4$ and $BA_2PbBr_4$ 2D perovskite hosts lattice, interstitial in the former and substitutional in the latter. Interestingly, the resultant crystal shows intense $Mn^{2+}$ emission, which is more efficient in $PEA_2PbBr_4$ compared to $BA_2PbBr_4$. The discrepancy in optical properties is most likely due to the nature of doping and its impact on the crystal lattice, including dopant-induced in-plane and out-of-plane lattice strain. Consequently, we observed a striking difference in the exciton diffusion. However, a few aspects like the interstitial site of $Mn^{2+}$ in crystal, the local structure around $Mn^{2+}$ at the interstitial site, and the role of organic spacers require further exploration.

## Data availability

The data supporting this article have been included as part of the ESI.†

## Conflicts of interest

There are no conflicts to declare.

## Notes and references

1 M. D. Smith, *et al.*, *Chem. Rev.*, 2019, **119**, 3104–3139.
2 Y. Li, *et al.*, *ChemComm*, 2022, **58**, 941–944.
3 A. J. Torma, *et al.*, *ACS Nano*, 2021, **15**, 20550–20561.
4 S. K. Dutta, *et al.*, *ACS Energy Lett.*, 2019, **4**, 343–351.
5 S. Hou, *et al.*, *Joule*, 2018, **2**, 2421–2433.
6 T. Sheikh and A. Nag, *J. Phys. Chem. C*, 2019, **123**, 9420–9427.
7 F. C. Grozema, *et al.*, *J. Phys. Chem. C*, 2020, **124**, 28201–28209.
8 C. Zhou, *et al.*, *Mater. Sci. Eng., R*, 2019, **137**, 38–65.
9 S. A. Cuthriell, *et al.*, *Adv. Mater.*, 2022, **34**, 2202709.
10 A. Biswas, *et al.*, *Chem. Mater.*, 2017, **29**, 7816–7825.
11 A. Khorsand Zak, *et al.*, *Solid State Sci.*, 2011, **13**, 251–256.
12 R. Kamal Yadav and P. Chauhan, *Indian J. Pure Appl. Phys.*, 2019, **57**, 881–890.
13 T. Jin, *et al.*, *Nat. Commun.*, 2023, **14**, 1–9.
14 D. B. Straus and C. R. Kagan, *J. Phys. Chem. Lett.*, 2018, **9**, 1434–1447.
15 C. M. Mauck and W. A. Tisdale, *Trends Chem.*, 2019, **1**, 380–393.
16 M. Seitz, *et al.*, *Nat. Commun.*, 2020, **11**, 1–8.